Potential Vorticity Diagnosis of a Simulated Hurricane. Part I: Formulation and Quasi-Balanced Flow

XINGBAO WANG AND DA-LIN ZHANG

Department of Meteorology, University of Maryland at College Park, College Park, Maryland

(Manuscript received 20 August 2002, in final form 27 January 2003)

ABSTRACT

Because of the lack of three-dimensional (3D) high-resolution data and the existence of highly nonelliptic flows, few studies have been conducted to investigate the inner-core quasi-balanced characteristics of hurricanes. In this study, a potential vorticity (PV) inversion system is developed, which includes the nonconservative processes of friction, diabatic heating, and water loading. It requires hurricane flows to be statically and inertially stable but allows for the presence of small negative PV. To facilitate the PV inversion with the nonlinear balance (NLB) equation, hurricane flows are decomposed into an axisymmetric, gradient-balanced reference state and asymmetric perturbations. Meanwhile, the nonellipticity of the NLB equation is circumvented by multiplying a small parameter ε and combining it with the PV equation, which effectively reduces the influence of anticyclonic vorticity. A quasi-balanced ω equation in pseudoheight coordinates is derived, which includes the effects of friction and diabatic heating as well as differential vorticity advection and the Laplacians of thermal advection by both nondivergent and divergent winds.

This quasi-balanced PV–ω inversion system is tested with an explicit simulation of Hurricane Andrew (1992) with the finest grid size of 6 km. It is shown that (a) the PV–ω inversion system could recover almost all typical features in a hurricane, and (b) a sizeable portion of the 3D hurricane flows are quasi-balanced, such as the intense rotational winds, organized eyewall updrafts and subsidence in the eye, cyclonic inflow in the boundary layer, and upper-level anticyclonic outflow. It is found, however, that the boundary layer cyclonic inflow and upper-level anticyclonic outflow also contain significant unbalanced components. In particular, a low-level outflow jet near the top of the boundary layer is found to be highly unbalanced (and supergradient). These findings are supported by both locally calculated momentum budgets and globally inverted winds. The results indicate that this PV inversion system could be utilized as a tool to separate the unbalanced from quasi-balanced flows for studies of balanced dynamics and propagating inertial gravity waves in hurricane vortices.

1. Introduction

Nonlinear balanced (NLB) models have been widely used in theoretical studies to help understand the fundamental dynamics of tropical cyclones. The earliest work could be traced back to Eliassen (1952) who developed an axisymmetric nonlinear balance model to investigate how a hurricane vortex evolves under the influence of latent heat release and surface friction. Subsequently, various types of NLB models have been developed to study the balanced characteristics of hurricane vortices (e.g., Sundqvist 1970; Challa and Pfeffer 1980; Shapiro and Willoughby 1982). Balanced dynamics is of particular interest to many researchers because it enables one to identify and follow significant flow features (in ''slow manifold'') in space and time.

Since the comprehensive review work of Hoskins et al. (1985), the potential vorticity (PV) concept has been frequently used for understanding the three-dimensional (3D) balanced dynamics of extratropical cyclones (e.g., Reed et al. 1992; Huo et al. 1999a), tropical cyclones (e.g., Schubert and Alworth 1987), and convectively generated midlevel mesovortices (Olsson and Cotton 1997; Trier and Davis 2002). The PV concept is attractive due to its conservative property in the absence of diabatic and frictional processes, and its invertibility principle with which a complete 3D flow could be diagnosed from a known PV distribution, given a balanced condition and appropriate boundary conditions. However, strong nonlinearity in the PV and NLB equations, when applied to mesoscale motion, makes it almost impractical to perform the PV inversion. After applying an ad hoc linearization, Davis and Emanuel (1991, hereafter referred to as DE91; and later refined by Davis 1992) were able to develop a PV inversion algorithm that allows for decomposition of the 3D PV field in a piecewise manner for extratropical cyclones. This ad hoc linearization appears to be necessary to absorb high-

Corresponding author address: Dr. Da-Lin Zhang, Department of Meteorology, University of Maryland, College Park, MD 20742.
E-mail: dalin@atmos.umd.edu

order nonlinear terms and facilitate the convergence of iterative calculations because their reference PV, determined from its climatological (i.e., temporal mean) value, and PV anomalies were at the same order of magnitude (e.g., see Zhang et al. 2002, their Fig. 6). Nevertheless, their PV inversion algorithm has successfully been used to diagnose the effects of condensational heating (Davis and Weisman 1994; Davis et al. 1996), the interaction of different PV anomalies (Huo et al. 1999a), the impact of removing upper-level perturbations on the surface extratropical cyclogenesis (Huo et al. 1999b), the influence of upper- and low-level PV anomalies on the movement (Wu and Emanuel 1995a,b), and the intensification of tropical cyclones (Molinari et al. 1998).

While DE91's algorithm has been successfully used by Wu and Emanuel (1995a,b) to diagnose hurricane movement and the storm's influence on its track, the PV anomalies associated with the hurricane vortex have to be excluded in assessing the hurricane's total advective flow due partly to the use of a climatological PV distribution as a reference state and partly to the sensitivity of their inversion results to the choice of the hurricane center. Motivated by weak asymmetries in the hurricane core, Shapiro (1996), and Shapiro and Franklin (1999) developed a PV inversion algorithm to study hurricane motion by decomposing the horizontal winds into symmetric (vortex) and asymmetric (environmental) components. Thus, the removal of hurricane vortices, as required by Wu and Emanuel (1995a,b), was avoided.

Based on the asymmetric balance (AB) theory of Shapiro and Montgomery (1993), Möller and Jones (1998) developed a PV inversion algorithm to study the evolution of hurricane vortices in a primitive-equation model, and later Möller and Shapiro (2002) used it to evaluate balanced contributions to the intensification of Hurricane Opal (1995) in a Geophysical Fluid Dynamics Laboratory (GFDL) model forecast. The AB theory reduces to Eliassen's formulation for purely axisymmetric flow. An advantage of the AB theory is that it provides little restriction on the magnitude of divergence (Montgomery and Franklin 1998; Möller and Shapiro 2002), as compared to the small divergence assumed in the NLB models. However, the validity of the AB theory depends on a nondimensional parameter, that is, $(D_\lambda^2/Dt^2)/(\overline{\eta}\,\overline{\xi}) \ll 1$, which is the ratio of the azimuthal to inertial frequencies in a symmetric vortex, where $D_\lambda/Dt = \partial/\partial t + V_t/r)\partial/\partial\lambda$, V_t is the mean tangential wind, and (r, λ) denotes the (radius, azimuth) axes of the cylindrical coordinates, and $\overline{\eta} = (f + \partial V_t/\partial r + V_t/r)$ is the vertical component of mean absolute vorticity and $\overline{\xi} = f + 2V_t/r$ is the inertia parameter. A scale analysis by Shapiro and Montgomery (1993) indicates that the validity of the AB theory requires the squared local Rossby number

$$R_n^2 = \frac{n^2 V_t^2/r^2}{\overline{\eta}\,\overline{\xi}} \ll 1,$$

when D_λ^2/Dt^2 is evaluated by the advective contribution $n^2V_t^2/r^2$, where n is the azimuthal wavenumber. This implies that the AB theory may not be very accurate for high wavenumber asymmetries, even though the above scaling may have somewhat overestimated the magnitude of D_λ^2/Dt^2, according to Möller and Montgomery (1999) and Möller and Shapiro (2002).

Despite the above-mentioned advantage of the AB theory, the NLB models or similar balance algorithms have been widely used, due to their relative simplicities, to diagnose the balanced flows associated with mesoscale convective systems, including intense hurricane vortices (McWilliams 1985; Zhang et al. 2001). Moreover, the divergent component of 3D flows may be obtained from the balanced winds through the quasi-balanced ω equation (Davis et al. 1996; Olsson and Cotton 1997). Nevertheless, all of the balance formulations mentioned above set PV to be a positive threshold value everywhere in order to satisfy an ellipticity requirement for finding a solution. In fact, PV is often not positive in the upper outflow layer of hurricanes where intense anticyclonic vorticity is present. In addition, because of the lack of high-resolution, high quality winds and thermodynamic data, most of the previous PV diagnostic studies focused on the broad-scale balance characteristics of hurricane vortices, and few studies have been performed to investigate the quasi-balanced asymmetric characteristics in the inner core regions of a hurricane.

In this study, a PV inversion system is developed, following DE91, but their ad hoc linearization is abandoned and the ellipticity requirement of the NLB equation is circumvented. This PV inversion system will then be tested using a high-resolution ($\Delta x = 6$ km) explicit simulation of Hurricane Andrew (1992) with the fifth-generation Pennsylvania State University–National Center for Atmospheric Research (PSU–NCAR) nonhydrostatic mesoscale model (i.e., MM5). Liu et al. (1997, 1999) have shown that the triply nested grid (54/1816 km) version of MM5 reproduces reasonably well the track, intensity, as well as the structures of the eye, eyewall, spiral rainbands, the radius of maximum wind (RMW), and other inner-core features as compared to available observations and the results of previous hurricane studies. Their simulation provides a complete dynamically and thermodynamically consistent dataset for us to examine the feasibility and accuracy of this PV inversion system in diagnosing the quasi-balanced asymmetric characteristics in the storm's inner-core regions.

The next section shows the derivation of the PV inversion system, including the PV, NLB, and ω equations in pseudoheight Z coordinates. The associated elliptic conditions will be discussed. Section 3 describes computational procedures of the inversion algorithm as applied to a model-simulated hurricane vortex. Section 4 presents the inverted (axisymmetric and asymmetric) results as verified against the model-simulated. Some balanced and unbalanced characteristics of hurricane

flows will be shown. A summary and concluding remarks will be given in the final section.

2. Formulation

a. Potential vorticity inversion equations

Because of the importance of water loading in hydrostatic balance in the eyewall (Zhang et al. 2000), it is appropriate to begin with a more general form of Ertel's PV that takes into account of the moisture and precipitation effects (see Schubert et al. 2001):

$$Q = \frac{1}{\rho}\boldsymbol{\eta}\cdot\nabla\theta_\rho, \tag{1}$$

where ρ is the total density consisting of the sum of the densities of dry air, airborne moisture (vapor and cloud condensate), and precipitation; $\boldsymbol{\eta} = 2\boldsymbol{\Omega} + \nabla\times\mathbf{V}$ is the absolute vorticity vector; and θ_ρ is the virtual potential temperature with the water loading effect included (see appendix A for its definition). Schubert et al. (2001) showed that if a flow is balanced, there exists an invertibility principle with Eq. (1) that could yield the balanced mass and wind fields from the spatial distribution of PV. In the present study, the NLB equation is used as our balance condition. To derive the NLB equation, the horizontal wind $\mathbf{V}_h$ is decomposed into nondivergent and irrotational components by defining a streamfunction Ψ, and a velocity potential X; that is,

$$\mathbf{V}_h = (u, v) = -\nabla\Psi\times\mathbf{k} + \nabla\mathrm{X} = \mathbf{V}_\Psi + \mathbf{V}_\mathrm{X}, \tag{2}$$

where $|\mathbf{V}_\mathrm{X}| \ll |\mathbf{V}_\Psi|$, and Ψ and X satisfy the following relations, respectively:

$$\nabla^2\Psi = \mathbf{k}\cdot\nabla\times\mathbf{V}_h = \zeta, \qquad \nabla^2\mathrm{X} = \nabla\cdot\mathbf{V}_h = D, \tag{3}$$

where ζ is the vertical component of relative vorticity, and D is the horizontal divergence. Given ζ and D, Ψ and X can be inverted from (3) with appropriate boundary conditions.

With the above definition, the NLB equation relating the horizontal wind to the mass field can be written as

$$\nabla_h^2\Phi = \nabla_h\cdot(F\nabla_h\Psi) + 2J\left(\frac{\partial\Psi}{\partial X}, \frac{\partial\Psi}{\partial Y}\right) + \nabla_h\cdot\mathbf{F}_r, \tag{4}$$

where the capital letters denote dimensional variables, ∇_h is a 2D (X, Y) gradient operator, Φ is the geopotential height, F is the Coriolis parameter, J is a Jacobian operator, and $\mathbf{F}_r$ represents the frictional force including the effects of the numerical diffusion and the planetary boundary layer (PBL). Equation (4) is generally valid when the divergent component $\mathbf{V}_\mathrm{X}$ is much weaker than the rotational component $\mathbf{V}_\Psi$. This relation could be applied to a flow with large curvature, provided that the Froude number and aspect ratio are small (McWilliams 1985). Note that for an axisymmetric vortex on an F plane, Eq. (4) reduces to the gradient wind balance (GWB) in the absence of friction. Previous observational and modeling budget studies showed that GWB is a good approximation to the azimuthally averaged winds above the PBL within a 10% error (Willoughby 1990; Zhang et al. 2001).

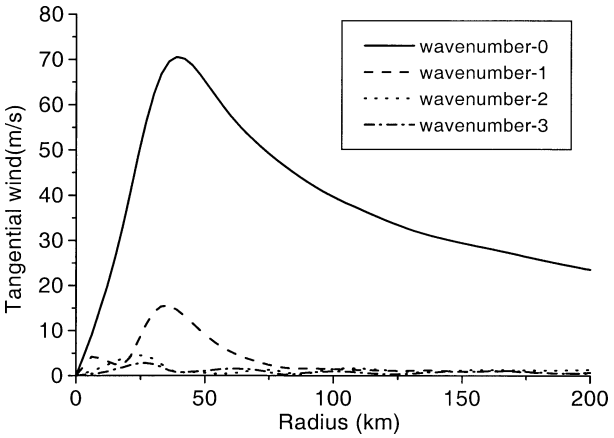

FIG. 1. Radial distribution of the wavenumber-0 (solid), wavenumber-1 (dashed), wavenumber-2 (dotted), and wavenumber-3 (dot-dashed) components of tangential winds at an altitude of 1 km, that are obtained by averaging 15 model outputs at 4-min intervals during the 1-h period from the 56–57-h simulation ending at 2100 UTC 23 Aug 1992.

Under the hydrostatic and nondivergent assumption, Eq. (1) can be rewritten as

$$Q = \frac{1}{r(Z)}\frac{\theta_0}{G}\left[(F + \nabla_h^2\Psi)\frac{\partial^2\Phi}{\partial Z^2} - \frac{\partial^2\Psi}{\partial X\partial Z}\frac{\partial^2\Phi}{\partial X\partial Z} - \frac{\partial^2\Psi}{\partial Y\partial Z}\frac{\partial^2\Phi}{\partial Y\partial Z}\right], \tag{5}$$

where $Z = [1 - (P/P_0)^{R/C_p}](C_p\theta_0/G)$ represents the vertical pseudoheight coordinate, G is dimensional gravitational acceleration, and $r(Z) = \rho_0(P/P_0)^{C_v/C_p}$ is pseudodensity (Hoskins and Bretherton 1972); see appendix A for a closed set of dynamical equations in Z coordinates used in this study. Given a PV distribution, Eqs. (4) and (5) are a closed set of equations in Φ and Ψ that may be solved iteratively to find a solution. However, several issues need to be considered before such a solution can be obtained.

First, Eqs. (4) and (5) could be highly nonlinear, depending on their applications, so a unique solution may not always be obtainable. Thus, it is desirable to linearize them by decomposing the total hurricane flow into a reference state and a perturbation component, as demonstrated by DE91 for extratropical cyclones. Prior to the decomposition, one should note that the balanced solution from Eqs. (4) and (5) requires the flow to be inertially and statically stable (Hoskins et al. 1985), but the snapshot model fields do not always satisfy the stability requirements. Therefore, to ensure the inertial and static stability of hurricane flow, we (a) set the vertical component of absolute vorticity η to be slightly positive (i.e., $\eta \geq 0.1f$); and (b) adjust the vertical θ_ρ structure

such that $\partial\theta_\rho/\partial Z \geq 0.01\ N^2\theta_0/G$ is always held, where N^2 ($=10^{-4}$ s^{-1}) is the buoyancy frequency, using the variational method of Sasaki and McGinley (1981). It is found that procedure (a) tends to be activated mostly in the upper outflow layer, whereas procedure (b) takes place mostly in the boundary layer and aloft in the eye. Of importance is that *the present procedures do not require* $Q > 0$ because of the possible existence of negative product of horizontal vorticity and θ_ρ gradient [see Eq. (5)]. However, after the above procedures, we did find that negative PV becomes weaker in the upper outflow layer and this tends to yield positive PV when it is azimuthally averaged.

To facilitate the subsequent discussions, it would be more convenient to rewrite Eqs. (4) and (5) in nondimensional form (see appendix B for more details); that is,

$$\nabla_h^2\phi = \boldsymbol{\nabla}_h\cdot(f\boldsymbol{\nabla}_h\psi) + 2J\left(\frac{\partial\psi}{\partial x},\frac{\partial\psi}{\partial y}\right) + \boldsymbol{\nabla}_h\cdot\mathbf{f}_r, \tag{4'}$$

$$q = \left[(f + \nabla_h^2\psi)\frac{\partial^2\phi}{\partial z^2} - \left(\frac{\partial^2\psi}{\partial x\partial z}\frac{\partial^2\phi}{\partial x\partial z} + \frac{\partial^2\psi}{\partial y\partial z}\frac{\partial^2\phi}{\partial y\partial z}\right)\right], \tag{5'}$$

where the lower cases denote nondimensionalized variables, unless mentioned otherwise hereafter. Note that each term in the above equations has one-to-one correspondence to that in Eqs. (4) and (5).

Because of the dominant axisymmetric nature of hurricanes, we decompose the hurricane flow fields into axisymmetric and its deviation (asymmetric) parts. In doing so, we first define the reference geopotential height $\overline{\phi}$ as its azimuthal average centered at the minimum surface pressure. The nondimensionalized reference variables $\overline{\psi}$ and $\overline{q}$ are then obtained from the GWB relation and Eq. (5′), respectively. An advantage of this procedure is that we do not need to iteratively solve Eqs. (4′) and (5′) for $\overline{\psi}$ and $\overline{\phi}$, given $\overline{q}$. [We have tried to calculate $\overline{\psi}$ first from the model output and then solved Eq. (4′) as Poisson equation for $\overline{\phi}$. But the resulting $\overline{\phi}$ leads to negative static stability near the top of the PBL where the tangential wind is peaked.] All the nondimentionalized perturbation variables are then obtained by

$$\psi' = \psi - \overline{\psi}, \qquad \phi' = \phi - \overline{\phi}, \quad \text{and}$$
$$q' = q - \overline{q}. \tag{6}$$

Figure 1 shows the radial distribution of azimuthally averaged tangential winds V_t (i.e., wavenumber 0) and their perturbation amplitudes V_t' in wavenumbers 1–3 at an altitude of 1 km where the tangential winds are nearly maximized. The tangential wavenumbers 1–3 winds are obtained after performing azimuthal Fourier decomposition in cylindrical coordinates. Obviously, the perturbation wind components are about one order of magnitude smaller than the azimuthal mean in the eyewall and outer regions (i.e., $\psi' \ll \overline{\psi}$, and $\phi' \ll \overline{\phi}$), unlike in the previous extratropical cyclogensis studies in which the reference and perturbation states were at the same order of magnitude when temporal means were used. Moreover, the higher the wavenumber, the smaller is the magnitude of perturbation winds. These results are similar to those shown in Shapiro and Montgomery (1993), and they also conform to the observational findings of Marks et al. (1992), Franklin et al. (1993), and Reasor et al. (2000) that the asymmetric components are less than 20% of the symmetric component. Thus, decomposing the total hurricane flow into the reference and perturbation components is consistent with the basic assumption involved in linearizing the nonlinear equations of (4′) and (5′), as given below.

Substituting (6) into Eqs. (4′) and (5′) gives

$$\begin{aligned}\nabla_h^2\phi' = {} & f\nabla_h^2\psi' + \beta\frac{\partial\psi'}{\partial y} \\ & + 2\left(\frac{\partial^2\overline{\psi}}{\partial x^2}\frac{\partial^2\psi'}{\partial y^2} - 2\frac{\partial^2\overline{\psi}}{\partial x\partial y}\frac{\partial^2\psi'}{\partial x\partial y} + \frac{\partial^2\psi'}{\partial x^2}\frac{\partial^2\overline{\psi}}{\partial y^2}\right) \\ & + 2\left[\frac{\partial^2\psi'}{\partial x^2}\frac{\partial^2\psi'}{\partial y^2} - \left(\frac{\partial^2\psi'}{\partial x\partial y}\right)^2\right] + \frac{\partial f_x}{\partial x} + \frac{\partial f_y}{\partial y},\end{aligned} \tag{7}$$

and

$$\begin{aligned}q' = {} & (f + \nabla_h^2\overline{\psi})\frac{\partial^2\phi'}{\partial z^2} + \nabla_h^2\psi'\frac{\partial^2\overline{\phi}}{\partial z^2} - \frac{\partial^2\overline{\psi}}{\partial x\partial z}\frac{\partial^2\phi'}{\partial x\partial z} \\ & - \frac{\partial^2\psi'}{\partial x\partial z}\frac{\partial^2\overline{\phi}}{\partial x\partial z} - \frac{\partial^2\overline{\psi}}{\partial y\partial z}\frac{\partial^2\phi'}{\partial y\partial z} - \frac{\partial^2\psi'}{\partial y\partial z}\frac{\partial^2\overline{\phi}}{\partial y\partial z} \\ & + \nabla_h^2\psi'\frac{\partial^2\phi'}{\partial z^2} - \frac{\partial^2\psi'}{\partial x\partial z}\frac{\partial^2\phi'}{\partial x\partial z} - \frac{\partial^2\psi'}{\partial y\partial z}\frac{\partial^2\phi'}{\partial y\partial z},\end{aligned} \tag{8}$$

where $\beta = \partial f/\partial y$. Although there are still a few nonlinear terms involving $\Pi(\psi', \phi')$ and $\Pi(\psi', \psi')$ on the right-hand side (rhs) of the above equations, they are one order of magnitude smaller than the linear terms, based on the results given in Fig. 1. Thus, the nonlinearity of Eqs. (7) and (8) is much weaker than that used to study extratropical cyclones. Furthermore, it can be readily shown that all these nonlinear terms will be absorbed if we follow DE91 by inserting $\psi^* = \overline{\psi} + 0.5\psi'$ and $\phi^* = \overline{\phi} + 0.5\phi'$ into Eqs. (7) and (8).

Second, if we solve (7) for ψ' with ϕ' obtained from (8), Eq. (7) is an elliptic equation of ψ' such that its associated elliptic condition must be met in order to find a solution (Arnason 1958). In the case of a stationary circular vortex, such a condition, given in cylindrical coordinates, can be written as

$$\left(f + 2\frac{V_t}{R}\right)\left(f + 2\frac{\partial V_t}{\partial R}\right) > 0. \tag{9}$$

The above criterion restricts the magnitude of anticyclonic shear vorticity $\partial V_t/\partial R$. Our calculations with the

simulated Andrew indicate that a sizeable area outside the RMW above the PBL is nonelliptic due to the presence of strong anticyclonic shear [i.e., $(f + 2(\partial V_t/\partial R)) < 0$]. To circumvent the ellipticity requirement, we multiply Eq. (7) by a parameter ε, varying between 0 and 1, and then add it into Eq. (8) to obtain

$$\left(\varepsilon f + \frac{\partial^2\overline{\phi}}{\partial z^2}\right)\nabla_h^2\psi' = q' - (f + \nabla_h^2\overline{\psi})\frac{\partial^2\phi'}{\partial z^2} + \frac{\partial^2\overline{\psi}}{\partial x\partial z}\frac{\partial^2\phi'}{\partial x\partial z} + \frac{\partial^2\psi'}{\partial x\partial z}\frac{\partial^2\overline{\phi}}{\partial x\partial z} + \frac{\partial^2\overline{\psi}}{\partial y\partial z}\frac{\partial^2\phi'}{\partial y\partial z} + \frac{\partial^2\psi'}{\partial y\partial z}\frac{\partial^2\overline{\phi}}{\partial y\partial z} - \nabla_h^2\psi'\frac{\partial^2\phi'}{\partial z^2} + \frac{\partial^2\psi'}{\partial x\partial z}\frac{\partial^2\phi'}{\partial x\partial z} + \frac{\partial^2\psi'}{\partial y\partial z}\frac{\partial^2\phi'}{\partial y\partial z} + \varepsilon\left[\nabla_h^2\phi' - \beta\frac{\partial\psi'}{\partial y} - 2\left(\frac{\partial^2\overline{\psi}}{\partial x^2}\frac{\partial^2\psi'}{\partial y^2} - 2\frac{\partial^2\overline{\psi}}{\partial x\partial y}\frac{\partial^2\psi'}{\partial x\partial y} + \frac{\partial^2\psi'}{\partial x^2}\frac{\partial^2\overline{\psi}}{\partial y^2}\right) - 2\left(\frac{\partial^2\psi'}{\partial x^2}\frac{\partial^2\psi'}{\partial y^2} - \frac{\partial^2\psi'}{\partial x\partial y}\frac{\partial^2\psi}{\partial x\partial y}\right) - \frac{\partial f_x}{\partial x} - \frac{\partial f_y}{\partial y}\right]. \quad (10)$$

Since the nonlinear terms $\Pi(\psi', \phi')$ and $\Pi(\psi', \psi')$ in the above equation are much smaller than the linear terms, we may assume the following elliptic condition for (10) approximately,

$$\left(\varepsilon f + 2\varepsilon\frac{\partial^2\overline{\psi}}{\partial x^2} + \frac{\partial^2\overline{\phi}}{\partial z^2}\right)\left(\varepsilon f + 2\varepsilon\frac{\partial^2\overline{\psi}}{\partial y^2} + \frac{\partial^2\overline{\phi}}{\partial z^2}\right) - 4\varepsilon\left(\frac{\partial^2\overline{\psi}}{\partial x\partial y}\right)^2 > 0. \quad (9')$$

where $\partial^2\overline{\phi}/\partial z^2 (=\overline{N}^2)$ is equivalent to the mean static stability. It is evident from (9′) that the value of ε to be used should be as small as possible, unless the atmosphere is very stable (e.g., in winter storms). However, ε cannot be too small due to its presence in the coefficient (i.e., εf) on the lhs of (10) in cases of weak static stability. In fact, we found that $\varepsilon = 0$ often leads to the divergence of iterative calculations, when solving for ψ' from (10), at points where the static stability is relatively weak or q' is large. On the other hand, when the vertical adjustment criterion of $\partial\theta_\rho/\partial Z \geq 0.2\, N^2\theta_0/G$ is used, any value of ε between 0 and 1 could result in a convergent solution. For the criterion chosen herein (i.e., $\partial\theta_\rho/\partial Z \geq 0.01\, N^2\theta_0/G$), the range of $\varepsilon = 0.1 \sim 0.8$ would yield a solution without encountering any nonellipticity problem. Thus, in this study a compromise value of $\varepsilon = 0.5$ is adopted to reduce the influence of anticyclonic shear vorticity on the elliptic requirement while enhancing the effects of static stability on the induced circulations associated with a given q' distribution.

Subtracting (8) from (7) leads to

$$\nabla_h^2\phi' + (f + \nabla_h^2\overline{\psi})\frac{\partial^2\phi'}{\partial z^2} = q' - \nabla_h^2\psi'\frac{\partial^2\overline{\phi}}{\partial z^2} + f\nabla_h^2\psi' + \beta\frac{\partial\psi'}{\partial y} + \frac{\partial f_x}{\partial x} + \frac{\partial f_y}{\partial y} - \nabla_h^2\psi'\frac{\partial^2\phi'}{\partial z^2} + \frac{\partial^2\overline{\psi}}{\partial x\partial z}\frac{\partial^2\phi'}{\partial x\partial z} + \frac{\partial^2\psi'}{\partial x\partial z}\frac{\partial^2\overline{\phi}}{\partial x\partial z} + \frac{\partial^2\overline{\psi}}{\partial y\partial z}\frac{\partial^2\phi'}{\partial y\partial z} + \frac{\partial^2\psi'}{\partial y\partial z}\frac{\partial^2\overline{\phi}}{\partial x\partial z} + \frac{\partial^2\psi'}{\partial x\partial z}\frac{\partial^2\phi'}{\partial x\partial z} + \frac{\partial^2\psi'}{\partial y\partial z}\frac{\partial^2\phi'}{\partial y\partial z} + 2\left(\frac{\partial^2\overline{\psi}}{\partial x^2}\frac{\partial^2\psi'}{\partial y^2} - 2\frac{\partial^2\overline{\psi}}{\partial x\partial y}\frac{\partial^2\psi'}{\partial x\partial y} + \frac{\partial^2\psi'}{\partial x^2}\frac{\partial^2\overline{\psi}}{\partial y^2}\right) + 2\left[\frac{\partial^2\psi'}{\partial x^2}\frac{\partial^2\psi'}{\partial y^2} - \left(\frac{\partial^2\psi'}{\partial x\partial y}\right)^2\right]. \quad (11)$$

Since perturbation variables are much smaller than their reference values, it is important to realize that the solution obtained from (10) and (11) is superposable to the reference state—an issue raised by Bishop and Thorpe (1994) and Thorpe and Bishop (1995).

Third, solving Eqs. (10) and (11) requires appropriate lateral, top and bottom boundary conditions. From the hydrostatic equation

$$\frac{\partial\phi}{\partial z} = \frac{g}{\theta_0}\theta_\rho, \quad (12)$$

Neumann boundary conditions for ϕ' can be specified at the bottom ($z = z_B$) and top ($z = z_T$) boundaries, respectively, as follows:

$$\left.\frac{\partial\phi'}{\partial z}\right|_{z=z_B} = \frac{g}{\theta_0}\theta'_{\rho B}; \qquad \left.\frac{\partial\phi'}{\partial z}\right|_{z=z_T} = \frac{g}{\theta_0}\theta'_{\rho T}. \quad (13)$$

Dirichlet boundary conditions for ψ' and ϕ' are specified along the lateral boundaries, where ϕ' matches the simulated or observed, and the tangential ψ' gradient matches the normal component of horizontal winds similar to that used by DE91. That is,

$$\frac{\partial\psi'}{\partial s} = -\mathbf{V}_h\cdot\mathbf{n} + \frac{\oint \mathbf{V}_h\cdot\mathbf{n}\, dl}{\oint dl}, \quad (14)$$

where l is a path along the lateral boundaries, $\mathbf{s}$ is a vector tangent to that path, and $\mathbf{n}$ a vector normal to

that path. Note that the domain-averaged net divergence, for example, resulting from the low-level inflow and upper-level outflow of hurricanes, must be deducted in order to satisfy the basic assumptions in deriving Eq. (7); so the second term is included on the rhs of Eq. (14). Of course, this term can be excluded when a large domain is used, for example, by Wu and Emanuel (1995a,b) and Shapiro (1996).

b. An ω equation for a quasi-balanced model

The PV inversion discussed above will yield 3D (nondivergent) balanced mass and horizontal wind fields that contain little vertical motion or secondary circulations of hurricanes. However, the secondary circulations, consisting of convergent inflow in the PBL, slantwise vertical motion in the eyewall, and divergent outflow in the upper troposphere, play an important role in determining the intensity of hurricane vortices and the development of clouds and precipitation in the eyewall. Clearly, any balanced theory of hurricanes would be incomplete without including the divergent wind component. However, including the divergent component to a balanced flow would differ from its conventional balance definition. In this regard, it would be more appropriate to consider the resulting total 3D flow as being quasi-balanced, because this divergent component associated with the balanced flow is presumably in ''slow manifold,'' unlike the divergent flow associated with gravity waves that tends to radiate away from energy sources.

Secondary circulations in hurricanes may result from the balanced flow (i.e., ψ and ϕ) and any dynamical and physical processes (e.g., friction $\mathbf{f}_r$ or diabatic heating $\dot{q}_\rho$), which can be determined by an ω equation and mass continuity equation, in a manner similar to their quasigeostrophic analog. To show this, we start from the vertical vorticity ζ equation

$$\frac{\partial \zeta}{\partial t} = -(\mathbf{V}_\psi + \mathbf{V}_\chi)\cdot\nabla_h\eta - \omega\frac{\partial \eta}{\partial z} - \eta\nabla_h\cdot\mathbf{V}_\chi + \frac{\partial \omega}{\partial y}\frac{\partial u}{\partial z} - \frac{\partial \omega}{\partial x}\frac{\partial v}{\partial z} + \frac{\partial f_y}{\partial x} - \frac{\partial f_x}{\partial y}, \tag{15}$$

and the thermodynamic equation

$$\frac{\partial \theta_\rho}{\partial t} + u\frac{\partial \theta_\rho}{\partial x} + v\frac{\partial \theta_\rho}{\partial y} + \omega\frac{\partial \theta_\rho}{\partial Z} = \dot{q}_\rho, \tag{16}$$

where ω is vertical velocity (positive implies upward motion) in pseudoheight z coordinates (see appendix A). Performing $(g/\theta_0)\nabla_h^2$ [Eq. (16)] $-$ ∂^2 [Eq. (4′)]/$\partial t\partial z$ $-$ $f\partial$ [Eq. (15)]/∂z, and after some manipulations, we obtain the following quasi-balanced ω equation

$$\nabla_h^2\left(\frac{\partial^2\phi}{\partial z^2}\omega\right) + f\eta\frac{\partial}{\partial z}\left\{(z_a - z)^{-\mu}\frac{\partial}{\partial z}[(z_a - z)^\mu\omega]\right\} - f\frac{\partial}{\partial z}\left(\frac{\partial \omega}{\partial x}\frac{\partial^2\psi}{\partial x\partial z} + \frac{\partial \omega}{\partial y}\frac{\partial^2\psi}{\partial y\partial z}\right) - f\frac{\partial}{\partial z}\left(\frac{\partial \omega}{\partial x}\frac{\partial^2\chi}{\partial y\partial z} - \frac{\partial \omega}{\partial y}\frac{\partial^2\chi}{\partial x\partial z}\right)$$
$$-\left(f\frac{\partial \eta}{\partial z}\frac{\mu}{z_a - z} + f\frac{\partial^2\eta}{\partial z^2}\right)\omega = f\frac{\partial}{\partial z}[\mathbf{V}_h\cdot\nabla\eta] - \nabla_h^2\left[\mathbf{V}_h\cdot\nabla_h\frac{\partial\phi}{\partial z}\right] - 2\frac{\partial^2}{\partial t\partial z}\left(\frac{\partial^2\psi}{\partial x^2}\frac{\partial^2\psi}{\partial y^2} - \frac{\partial^2\psi}{\partial x\partial y}\frac{\partial^2\psi}{\partial x\partial y}\right) - \beta\frac{\partial^3\psi}{\partial t\partial y\partial z}$$
$$+ \frac{g}{\theta_0}\nabla_h^2\dot{q}_\rho - f\frac{\partial}{\partial z}\left(\frac{\partial f_y}{\partial x} - \frac{\partial f_x}{\partial y}\right) - \frac{\partial^2}{\partial t\partial z}\left(\frac{\partial f_x}{\partial x} + \frac{\partial f_y}{\partial y}\right), \tag{17}$$

where $\mu = C_v/R_d$, ψ, and ϕ are the total streamfunction and geopotential height. The dimensional form of Eq. (17) is similar to that derived by Krishnamurti (1968) and DE91 except for the use of z coordinates and inclusions of the velocity potential χ, and the frictional and water loading effects. Apparently, the vertical motion of the quasi-balanced model can be determined by the rhs forcing terms of Eq. (17), which, from the left to right, are the differential vorticity advection and the Laplacians of thermal advection both by nondivergent and divergent winds, the differential deformation or Jacobian term, the β effect, latent heating, and the effects of friction, respectively. The first four forcing terms are more dynamically related and diagnosed from the NLB–PV equation model; in these four terms, divergent winds also play an important role in advecting various flow properties (Raymond 1992). The last three terms are more physically related and the major sources in determining the magnitude of divergent winds and secondary circulations in hurricanes, which will, in turn, contribute to the intensities of the first four dynamic forcing terms.

Apparently, Eq. (17) is not a fully diagnostic equation because of the existence of two local tendency terms; that is, we must know $\partial\psi/\partial t$, $\partial f_x/\partial t$, and $\partial f_y/\partial t$ in order to find ω. The term $\partial\psi/\partial t$ could be obtained by either solving Eq. (15), like in Krishnamurti (1968), or taking a time derivative of Eqs. (4) and (5), like in DE91; the former approach is adopted here. The frictional terms of $\partial f_x/\partial t$ and $\partial f_y/\partial t$ are obtained directly from the model output.

Because of an additional variable χ included in Eq.

(17), which will give the divergent, radial component of hurricane vortices, we need to introduce the continuity equation

$$\nabla^2\chi = -(z_a - z)^{-\mu}\frac{\partial}{\partial z}[(z_a - z)^{\mu}\omega]. \qquad (18)$$

Thus, if the diabatic and frictional contributions are known (e.g., from a model simulation), Eqs. (15), (17), and (18) form a closed set of equations in ω, χ, and $\partial\psi/\partial t$.

In summary, the two sets of equations [i.e., Eqs. (10), (11) and (15), (17), (18)] plus the reference state define completely a 3D quasi-balanced flow field (both nondivergent and divergent) through ψ, χ, and ω, and a quasi-balanced mass field through ϕ. From these quantities, all the other relevant balanced properties of the fluid system (e.g., temperature) can be deduced. Since the two sets of equations are in forcing and response mode, the piecewise partitioning and inversion could be in principle conducted to gain insight into the impact of various isolated PV perturbations or different physical processes on hurricane flows.

3. Computational procedures

To demonstrate how well the inner-core quasi-balanced mass and winds of a hurricane could be inverted from a given PV distribution using the algorithm developed in the preceding section, the model-simulated Hurricane Andrew (1992) data are output over the two fine-mesh (18 and 6 km) domains at 4-min intervals from the 56–57-h integration, valid at 2000–2100 UTC, 23 August 1992. During this period, the storm has entered its mature stage with a (near steady) maximum surface wind of 68 m s^{-1}, although its central pressure is still decreasing at a rate of 1 hPa h^{-1} (see Liu et al. 1997, their Fig. 2). All the snapshot mass and wind fields, as well as the forcing (diabatic and friction) and local tendency terms, are then decoupled from their MM5 flux forms.

To reduce the influence of lateral boundaries on the final solution [e.g., see Eq. (14)], the finest (6 km) resolution domain is extended in the y direction by interpolating the intermediate (18-km resolution) mesh data, leading to the (x, y) dimensions of 124 × 124 points covering a horizontal area of 738 km × 738 km. The model data are then interpolated in the vertical from MM5's 23 uneven σ layers to 34 even z coordinates layers to facilitate the PV inversion using the multigrid solver MUDPACK of Adams (1993). Note that the 34 (even) layers could not retain the original high vertical resolution model data in the PBL. As will be seen in the next section, the reduced vertical resolution tends to misrepresent somewhat the boundary layer frictional effects; see Liu et al. (1997, 1999) for a detailed description of the model configurations.

To decompose the simulated hurricane flow into a reference (axisymmetric) state and a perturbation state, all the 3D data are transformed from the (x, y, z) to the cylindrical (r, λ, z) coordinates with its origin defined at the minimum sea level pressure of the storm, following the procedures described in Liu et al. (1999), and then averaged azimuthally to yield the GWB reference state. All the reference and perturbation variables are nondimensionalized. With 3D perturbation PV (q') from the model output, Eqs. (10) and (11) are iteratively solved, subject to the boundary conditions (13) and (14), for the perturbation mass and winds; the results are then added to their reference state. After obtaining the balanced total mass and winds, Eqs. (15), (17), and (18) are iteratively solved with the diabatic and frictional forcing terms from the model output. In doing so, we define P = 980 hPa as the bottom boundary in the present z coordinates, which puts the eye region (with the minimum central pressure of less than 925 hPa) essentially above the sea surface. Clearly, in this situation, it is not appropriate to specify $\omega = 0$ as the bottom boundary condition. Thus, the mass continuity equation (18) is integrated from the model top downward, following Olsson and Cotton (1997), assuming $\omega|_{z=z_r} = 0$. Finally, all the inverted fields are averaged temporally over a 1-h period, and then compared to the hourly averaged model outputs that are similar in magnitude and structure to those shown in Liu et al. (1999) and Zhang et al. (2001).

4. Quasi-balanced flow

In this section, the quasi-balanced hurricane mass and wind fields are inverted with the PV inversion system developed in section 2, and then verified against the model simulated in both the west–east and the azimuthally averaged radius–height cross sections, in order to examine its capability in representing the quasi-balanced, asymmetric and axisymmetric structures of inner-core flows. Figure 2 compares the simulated PV and in-plane flow vectors to the inverted in west–east vertical cross sections. Pronounced asymmetries of the eyewall and its associated flow features are apparent (Fig. 2a). For example, the western eyewall is characterized by more intense upward motion and upper-level outflow with a deeper secondary circulation than those in the east. This is consistent with the development of more intense deep convection and precipitation in the west semicircle (see Liu et al. 1997, their Fig. 5b). Of interest is the concentration of high PV (over 40 PVU; 1 PVU = 10^{-6} m^2 K kg^{-1} s^{-1}) in the eye where little latent heating occurs; it coincides with the location of an intense thermal inversion layer near z = 2.5 km. This feature will have to be studied through PV budget calculations and it will be reported in a future article. Of further interest is the development of a U-shaped PV structure above the warm core (i.e., near z = 6 km) that appears to result from the cyclonic slantwise upward advection of the high PV associated with latent heat release in the eyewall and the slow cyclonic downward

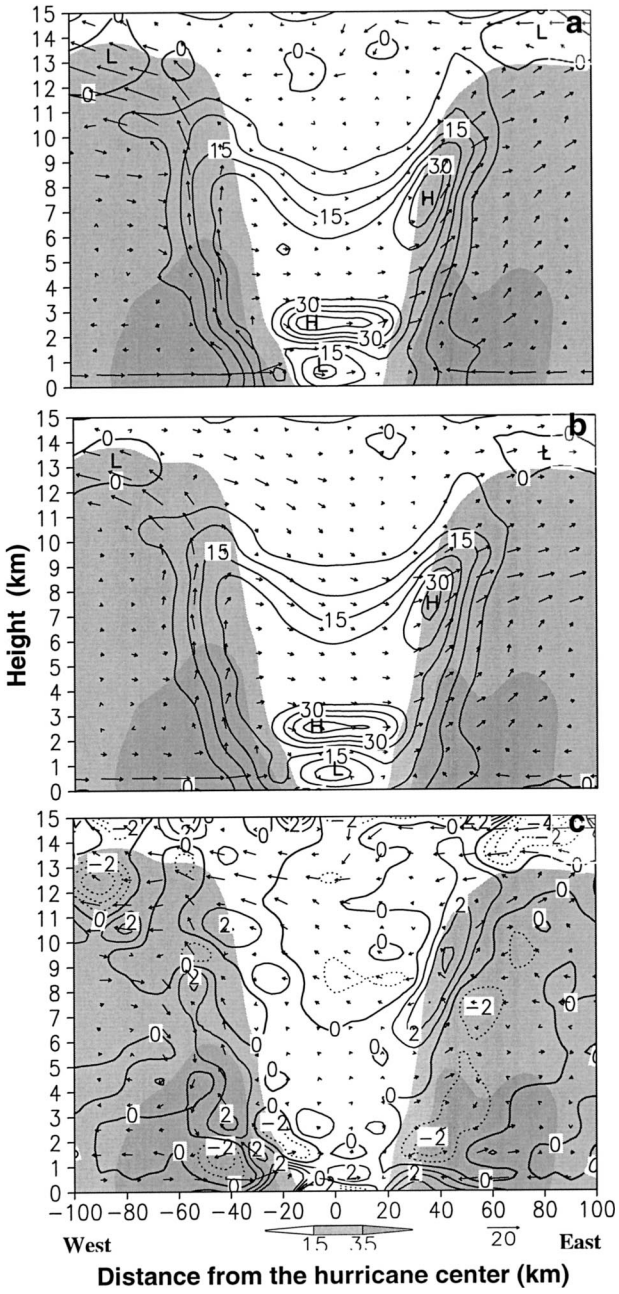

FIG. 2. West–east vertical cross sections of PV (contoured), superposed with storm-relative in-plane flow vectors, from (a) the model output (every 5 PVU), (b) the inverted or recalculated (every 5 PVU), and (c) the differences (every 0.5 PVU) between (a) and (b) [i.e., (a) minus (b)]. They are obtained by averaging 15 datasets at 4-min intervals during the 1-h period ending at 2100 UTC 23 Aug 1992. Shadings denote the simulated radar reflectivity greater than 15 and 35 dBZ, which represents roughly the distribution of precipitation with two different intensities. Solid (dashed) lines are for positive (negative) values. Note that vertical velocity vectors have been amplified by a factor of 5.

advection of low PV in the eye. Negative PV is visible in the upper-level outflow where anticyclonic vorticity is large.

It is encouraging from Figs. 2b and 2c that the recalculated PV from the inverted mass and wind fields and the inverted in-plane flows compare favorably to the simulated, including the magnitude and distribution of PV, and the storm's secondary circulations. In particular, the peak PV in the eye's inversion layer (and another PV center below), which appears to dominate the hurricane vortex, is well recovered, indicating the great capability of this inversion technique in recovering the hurricane flows. However, some differences in the PBL and the upper outflow layer are notable. They could be attributed partly to the use of reduced vertical resolution (i.e., in representing the frictional effects) and of the required nonnegative absolute vorticity and larger static stability, respectively. Nevertheless, the upper-level anticyclonic outflow might be in a transition stage in case symmetric instability (i.e., PV < 0) is operative.

Figure 3 compares the inverted primary circulation of the hurricane to the simulated. Evidently, the PV inversion recovers the basic structures and magnitudes of the hurricane's tangential flows, such as weak flows in the eye, intense asymmetric wind maximums (over 65 m s^{-1}) near the top of the PBL, decreasing winds in the PBL, and the slantwise sloping RMW with large negative vertical shears in the eyewall (cf. Figs. 3a,b). As simulated, the inverted RMW axis is also situated outside of the updraft core. However, the globally inverted fields are generally smoother than the simulated (e.g., wavy isotachs and locally reversed vertical shears near $z = 2$ km and $R = 40$ km), as expected. Again, more notable differences appear in the PBL where the dynamic unbalance is more pronounced due partly to the surface friction and partly to the previously mentioned inaccurate representation of the frictional effects, and in the upper levels where the inverted flows are more constrained by rotational dynamics due to the requirement of nonnegative absolute vorticity (Fig. 3c). In addition, slightly stronger tangential flows (± 5 m s^{-1}) are inverted in the vicinity of the eye–eyewall interface where significant downdrafts appear. Despite the stated limitations and some possible inversion and interpolation errors, most of these differences could be considered as the unbalanced component of the hurricane flows, especially for the layers above the PBL where the differenced field is relatively small.

Of significance is that the unbalanced tangential winds become much weaker after the azimuthal average (see Fig. 4c), suggesting that most of them may be associated with inertial gravity waves as those shown by Liu et al. (1999) since the magnitudes of other possible waves (e.g., acoustic) are small. This remains a subject for future study. In particular, the inverted radius–height distribution of tangential flows compares extremely well with the simulated (cf. Figs. 4a,b). The globally inverted unbalanced flows (i.e., ± 2–4 m s^{-1}), though differing

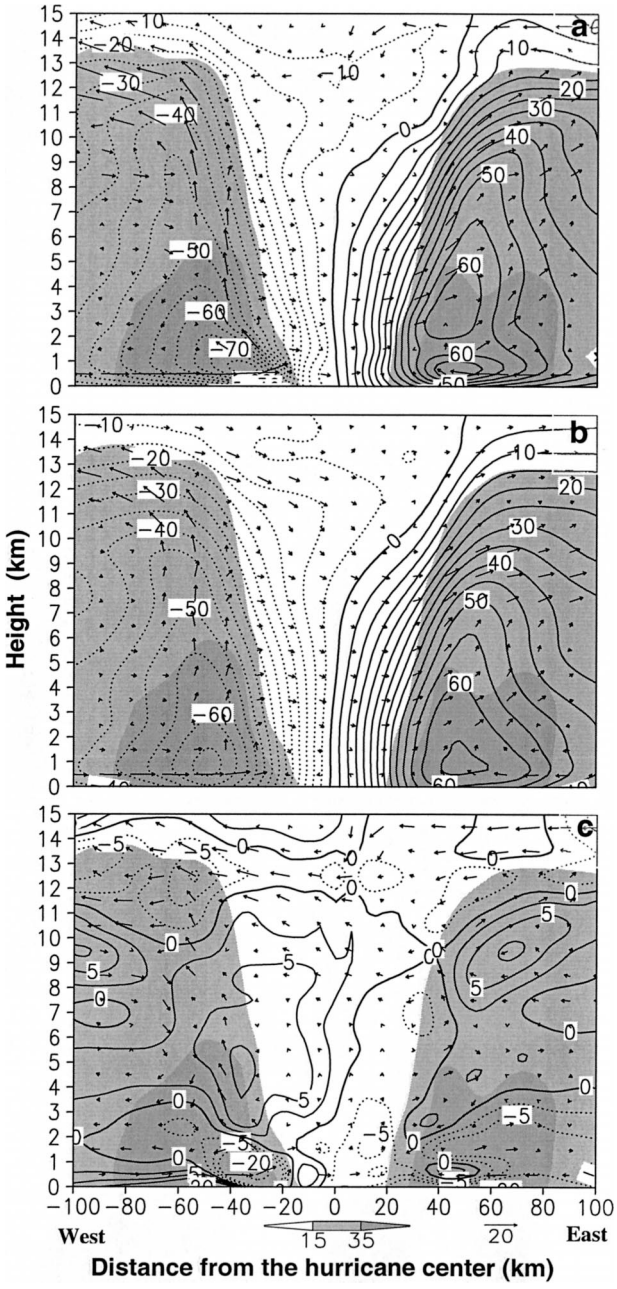

FIG. 3. As in Fig. 2, but for tangential winds contoured at intervals of (a), (b) 5 m s^{-1}; and (c) contoured at 0, ±2.5, ±5, ±7.5, and ±20 m s^{-1}. Solid (dashed) lines denote tangential flows [in (a) and (b)] or their differenced flows [in (c)] into (out of) the page.

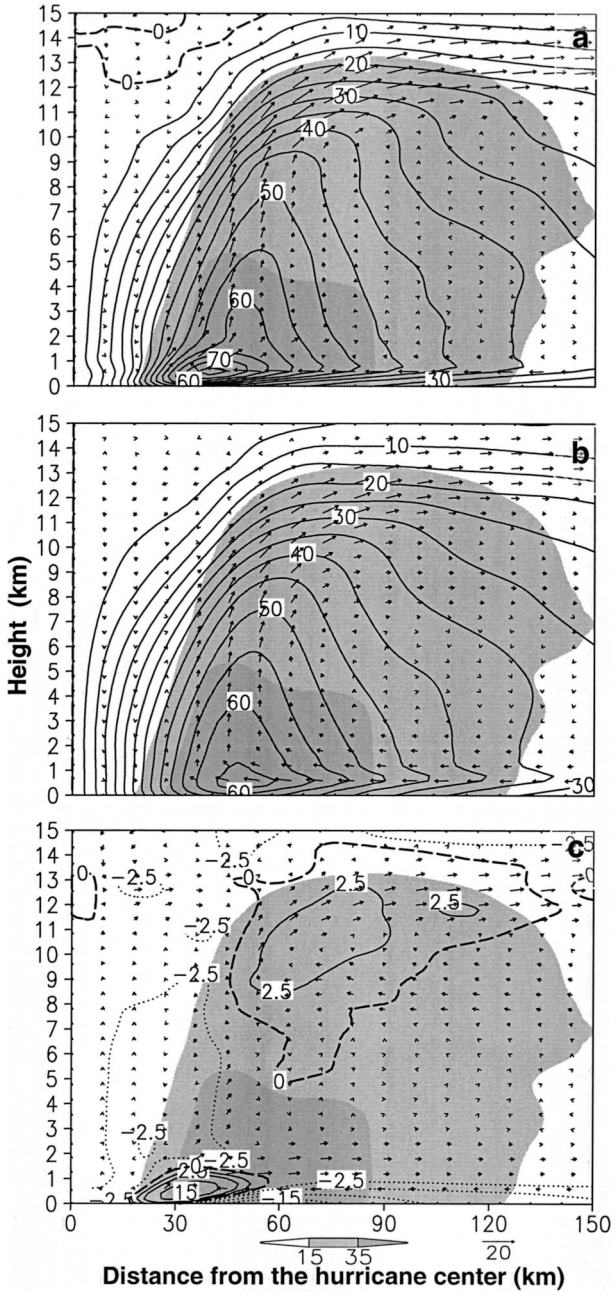

FIG. 4. As in Fig. 3, but for height–radius cross sections of tangential winds within the radius of 150 km. Note that (c) isopleths are given at 0, ±2.5, ±5.0, ±10, and ±15 m s^{-1}.

in structure, are also similar to the locally derived agradient winds above the PBL (cf. Fig. 7 in Zhang et al. 2001 and Fig. 4c herein). These results all indicate that *the azimuthally averaged tangential flows above the PBL are approximately in GWB,* conforming to the observational analysis of Willoughby (1990) and the momentum budget study of Zhang et al. (2001). The inverted large positive (negative) unbalanced tangential winds (about 12 m s^{-1}) associated with a low-level radial outflow jet are also consistent with those (about 16 m s^{-1}) shown in Zhang et al. (2001, cf. their Fig. 7b, and Fig. 4c herein). We speculate that this unbalanced component would be much weaker if the mass field is forced toward the wind field. That is, the reference state $\overline{\psi}$ is calculated first and then Eq. (4′) is solved as Poisson equation for $\overline{\phi}$. As mentioned earlier, this procedure tends to generate statically unstable lapse rates near the top of the PBL.

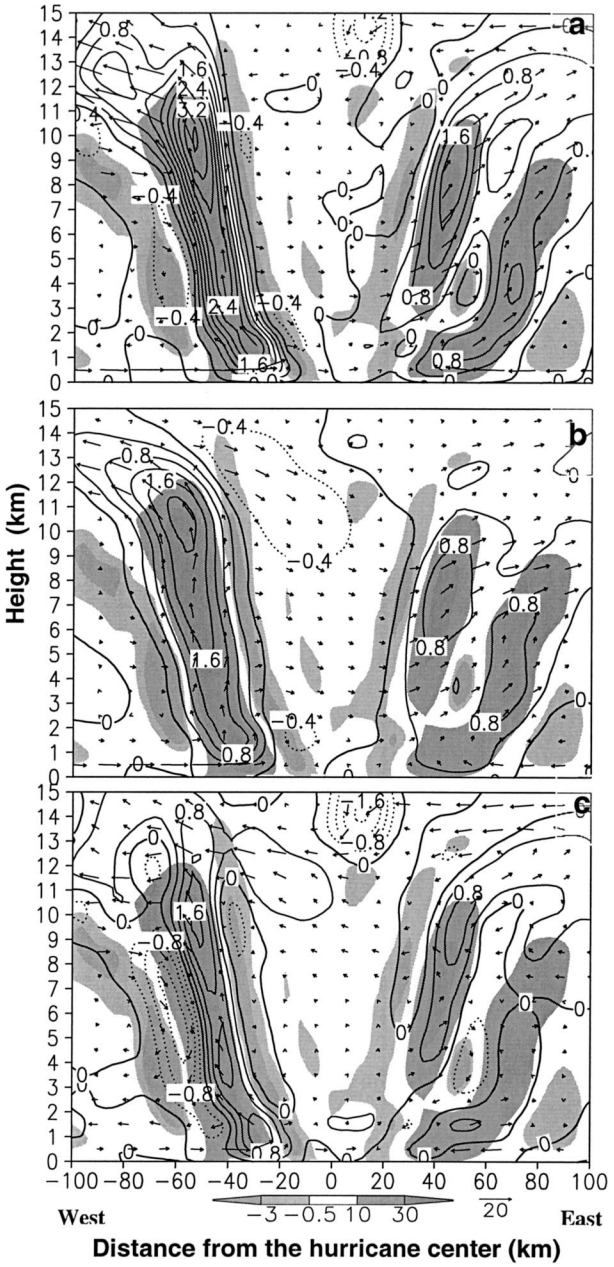

FIG. 5. As in Fig. 2, but for vertical motion at intervals of 0.4 m s^{-1}. Dark shadings denote latent heating rates greater than 10 and 30 K h^{-1}, whereas light shadings denote latent cooling rates less than −0.5 and −3 K h^{-1}.

The inverted secondary circulations from the quasi-balanced ω equation (17) are compared to the simulated in Fig. 5, which shows well the development of deep, boundary-layer-rooted and shallow, ''suspended'' slantwise updrafts in the western and eastern eyewall, respectively. Of significance is that both the inverted and simulated vertical motion bands are almost *in phase* with latent heat release, especially in the eyewall and major rainbands where more intense latent heating occurs. The inverted maximum updrafts are about 2.0 and 1.0 m s^{-1} in the respective western and eastern eyewall, as compared to the simulated 3.5 and 1.6 m s^{-1} (cf. Figs. 5a,b), indicating that *about 60%–70% of peak updrafts in the eyewall are quasi-balanced.* The updraft and downdraft bands in the outer regions are also reasonably recovered, albeit with different intensities from the simulated. Thus, we may state that the quasi-balanced ω equation can recover reasonably the vertical motion field of a hurricane for either diagnostic analyses or model initialization, given 3D latent heating and friction along with its vortex flow. After all, vertical motion in hurricanes represents the response of a primitive equation or balanced model to diabatic heating and the PBL effects.

Of importance is that the Laplacians of latent heating in the eyewall and other dynamical processes, as shown in Eq. (17), yield general (balanced) subsidence in the eye where little physics forcing occurs. However, the upper-level subsidence appears to be overestimated, as compared to the simulated; this is consistent with the reduced anticylonic outflow and the increased return flow into the eye in the inverted fields (cf. Figs. 5b and 3c). In contrast, the pronounced downdrafts, originating from the upper-level return flow and coinciding with the evaporative cooling at the eye–eyewall interface, do not appear in the inverted field (cf. Figs. 5a,b). This might be a result of the horizontal resolution used (i.e., $\Delta x =$ 6 km) that is too coarse for the model integration and PV inversion to resolve the interface downdrafts radially. On the other hand, these narrow downdrafts are found to be driven mostly by cold advection in radial inflow (see Zhang et al. 2002), so they are not deemed to be possibly inverted from the given weak cooling rates. Of further importance is that propagating gravity waves shown in Liu et al. (1999, see their Fig. 8) are completely absent in Fig. 5b or at any other time (not shown). Instead, these waves appear in the differenced ω field, in both the inner core and outer regions (Fig. 5c); some ω bands are 90° out of phase with the latent heating. These bands are unbalanced by definition and must be consistent with their pertinent unbalanced wind and mass fields.

Figure 6 compares the height–radius cross sections of azimuthally averaged, inverted vertical motion to the simulated. Again, the ω equation reproduces a robust updraft in the eyewall and general subsidence in the eye (cf. Figs. 6a,b). Although there are notable differenced updraft centers in the eyewall (Fig. 6c), more than 65% of the peak axisymmetric eyewall updraft intensity is quasi-balanced. By comparison, the quasi-balanced ω bands in the outer regions vanish after azimuthal average (cf. Figs. 6b and 5b), suggesting that they are highly asymmetric. Unbalanced axisymmetric ω bands also show some evidence of propagating gravity waves, especially in the vicinity of the eyewall (Fig. 6c), suggesting that the eyewall may be the energy source of inertial gravity waves.

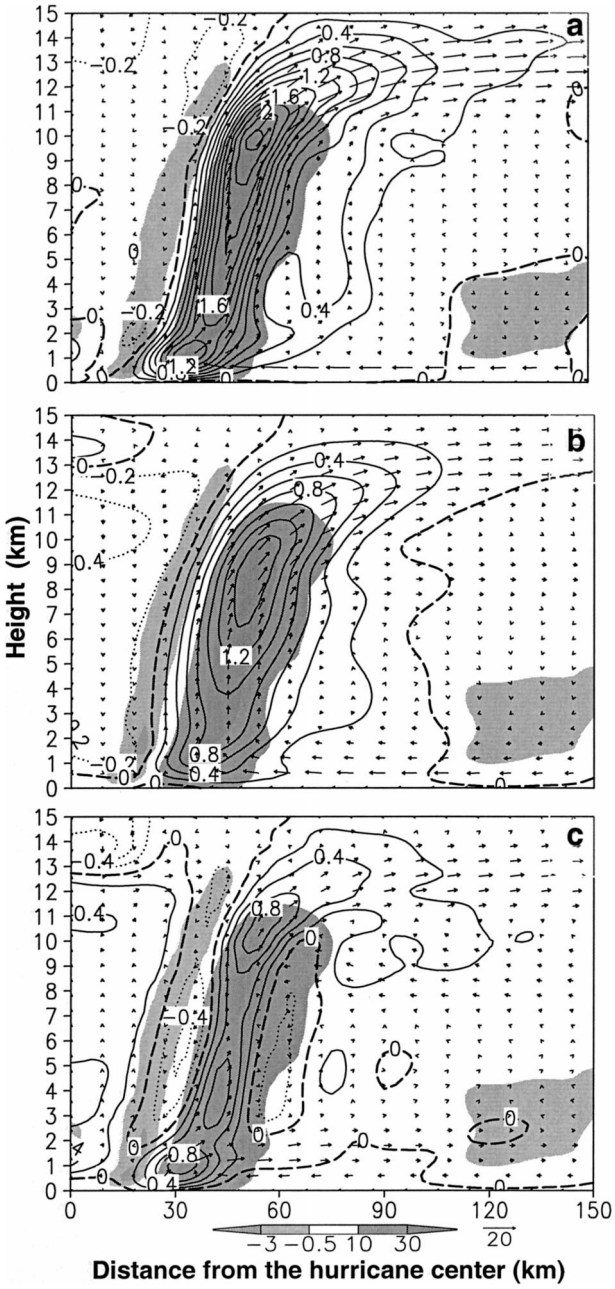

FIG. 6. As in Fig. 5, but for height–radius cross sections of vertical motion at intervals of 0.2 m s^{-1} within the radius of 150 km.

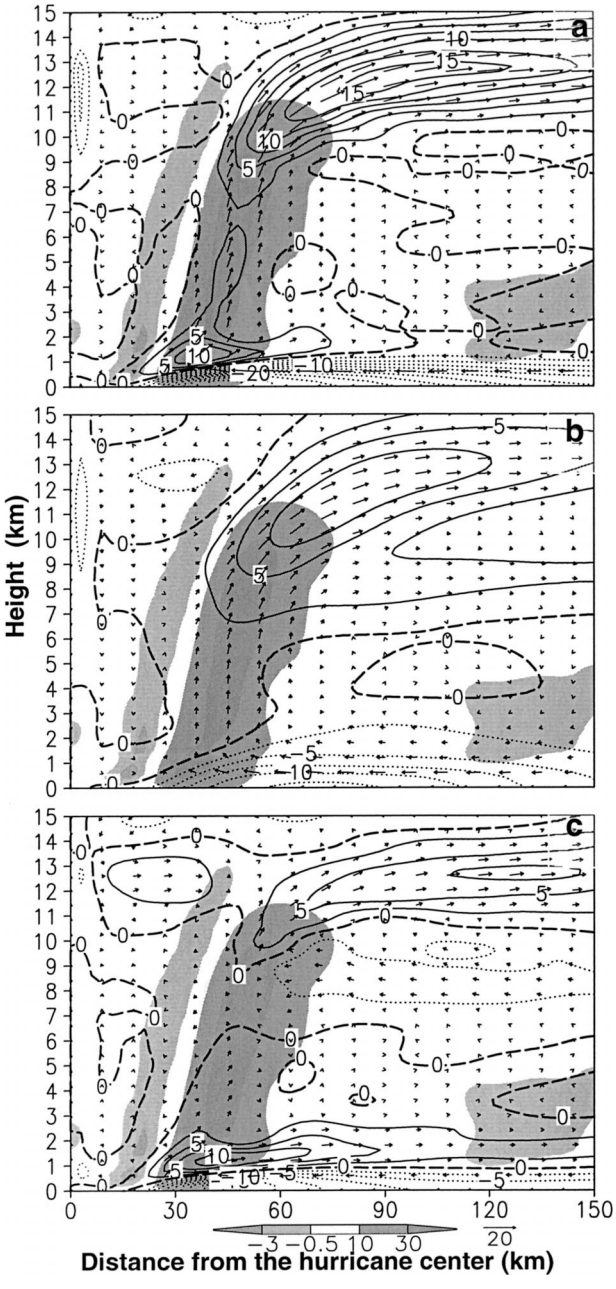

FIG. 7. As in Fig. 2, but for height–radius cross sections of radial winds at intervals of 2.5 m s^{-1} within the radius of 150 km. Solid and dashed lines denote radial outflow and inflow, respectively.

It is apparent from Fig. 7 that the PV inversion system reproduces reasonably well a general radial inflow in the lowest 2 km from the outer to inner-core regions, and a radial outflow, which is supergradient (Zhang et al. 2001), from the bottom eye to the upper-level outflow (cf. Figs. 7a,b). As discussed in Zhang et al. (2001), the supergradient outflows result from the rapid upward transport of absolute angular momentum such that the local centrifugal force exceeds the radial pressure gradient force. The radial outflows tend to spin down a cyclone's intensity. However, the inverted radial flows appear to ''underestimate'' the simulated systematically (Fig. 7c). In particular, the azimuthally averaged low-level outflow jet associated with the Ekman pumping (Willoughby 1979) is quite weak; it is instead replaced by a deep radial inflow. As discussed in Liu et al. (1999) and Zhang et al. (2001, 2002), this outflow jet plays an important role in transporting high-θ_e air from the eye to support deep convection in the eyewall and in drawing air out of the eye to reduce the central pressure. The

underestimated outflow jet and convergent inflow in the PBL explain why weaker upward motion in the lowest 1–2-km layer of the eyewall is obtained (cf. Figs. 5c and 7c). Nonetheless, the inverted and simulated radial flow differences are consistent with the unbalanced tendencies obtained by Zhang et al. (2001), so they could be treated as unbalanced radial flows. Specifically, their locally calculated radial momentum budget shows the presence of supergradient tendencies (a) in the eyewall from the bottom of the eye center to the upper outflow layer, (b) in association with the low-level outflow jet, (c) with the upper-level return inflow in the eye, and (d) the presence of subgradient tendencies in the lowest 1-km airflows outside the RMW (cf. their Figs. 6f and 7c herein). Apparently, radial flows exhibit a more significant portion of unbalanced component than tangential and vertical flows (cf. Figs. 4c, 6c, and 7c), since the radial outflows (inflows) represent a cross-isobaric component of hurricane flows, pointing toward higher (lower) pressures. Figure 7b shows that *about 50% of radial (cross isobaric) flows could be considered quasi balanced.*

Finally, we compare in Fig. 8 the inverted virtual potential temperature deviations θ'_ρ to the simulated. All deviations are obtained by subtracting their azimuthally and radially averaged values at individual heights. The inverted θ'_ρ shows an intense warm core and an intense inversion near $z = 3$ km in the eye, and strong thermal gradients across the sloping eyewall, which are all similar to the simulated. The inverted θ'_ρ is 2–5 K warmer than the simulated in the lowest 1–2 km of the eyewall, as can also be seen from decreased θ'_ρ curvatures (cf. Figs. 8a,b). This warmer boundary layer is attributable to the inverted weaker upward motion causing less adiabatic cooling and the inverted weaker inflow and outflow couplet near the top of the PBL (cf. Figs. 5c, 7c, and 8c). Otherwise, the total mass field is extremely well recovered, indicating that *unbalanced mass perturbations above the PBL are indeed small.* The small mass perturbations appear to be the characteristics of propagating gravity waves.

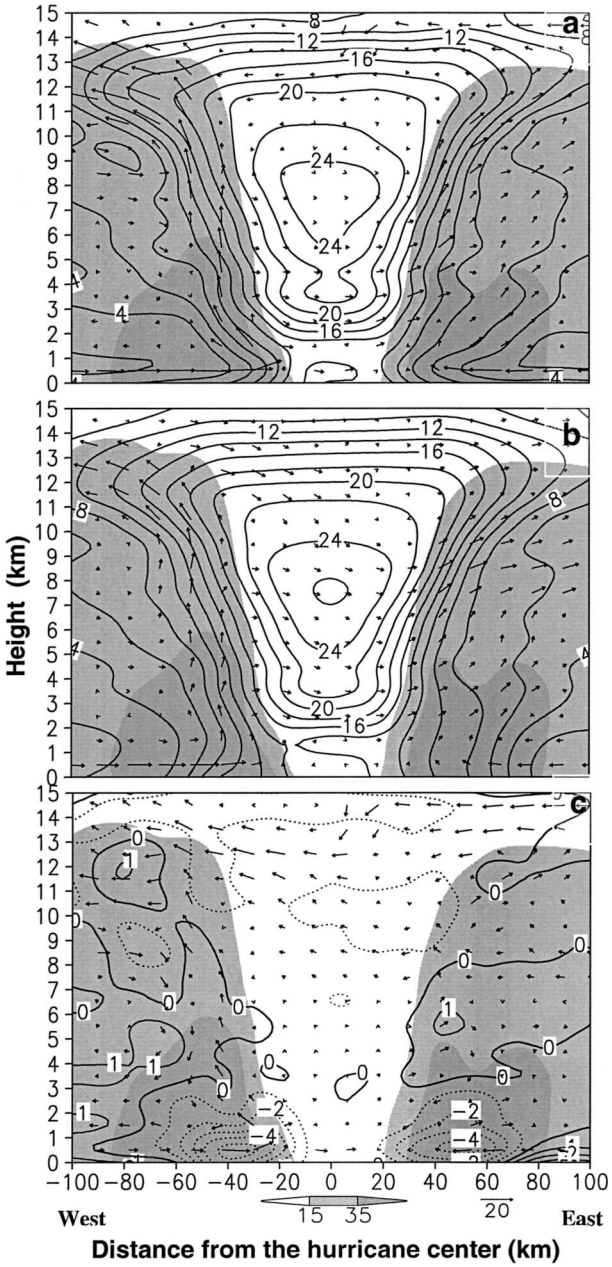

FIG. 8. As in Fig. 2, but for potential temperature deviations θ'_ρ at intervals of (a), (b) 2°C, and at intervals of (c) 1°C.

5. Summary and conclusions

In this study, a PV inversion system in pseudoheight Z coordinates has been derived for hurricane flows, following DE91, and then tested using an explicit simulation of Hurricane Andrew (1992) with the finest grid size of 6 km (Liu et al. 1997, 1999). This PV inversion system also includes the nonconservative effects of friction in the PBL, diabatic heating, and water loading in deep convection. It requires hurricane flows to be statically and inertially stable but allows for the presence of negative PV, thus reducing the extent of data modification. In order to better linearize the NLB–PV equations, azimuthally averaged (axisymmetric) flows in GWB are defined as a reference state and the remaining portions as perturbations. Since hurricane vortices are to some extent highly axisymmetric, DE91's ad hoc linearization assumption is abandoned and the so-obtained perturbation solution can be superposed onto the reference state to recover the balanced nondivergent winds and associated mass fields. To circumvent the high nonellipticity associated with intense anticyclonic shear vorticity that often occurs outside the RMW and in the upper outflow layers, a small parameter ε (=0.5) is introduced into the NLB equation that is then combined with the PV equation. This small parameter is used to reduce the influence of anticyclonic contribution while

enhancing the effects of static stability on the induced circulations associated with a given q' distribution. Divergent winds are obtained via the quasi-balanced ω equation with the inverted balance flow as input, assuming that the 3D distribution of diabatic heating, PBL effects, and hurricane vortices are known.

It is shown that the PV inversion system could recover well many of the typical features occurring in a hurricane, given 3D PV, boundary conditions and all the physics forcings. They include intense (subgradient) convergent inflow in the PBL and maximum tangential winds near its top, sloping RMW located outside the updraft ridge axis with supergradient flows in the eyewall, a low-level thermal inversion and a warm-cored eye with intense thermal gradients across the eyewall, organized updrafts in the eyewall and subsidence in the eye, and upper-level anticyclonic-divergent outflow.

However, the PV inversion system appears to underestimate the bottom cyclonic inflows, the Ekman pumping-induced upward motion and thermal perturbations in the PBL, and anticyclonic outflow in the upper levels. Although the use of coarser vertical resolution in representing the frictional effects and the required nonnegative absolute vorticity may have contributed to some of the underestimated magnitudes, a significant portion of their differences from the simulated could be treated as unbalanced. Relatively speaking, a more significant portion ($\approx$50%) of radial flows appears to be unbalanced, since the radial outflows (inflows) represent a cross-isobaric component of hurricane flows, pointing toward higher (lower) pressures. In particular, the low-level outflow jet, containing little quasi-balanced component, is highly supergradient and unbalanced. All these findings are well supported by both locally calculated momentum budgets and globally inverted winds.

Despite the presence of more significant unbalanced radial flows, the inverted and simulated mass and wind differences are found to be generally small above the PBL, particularly after their azimuthal averages. Thus, we may conclude that (a) 3D hurricane flows are to a certain extent quasi-balanced, including the intense rotational winds, organized eyewall updrafts and subsidence in the eye, cyclonic inflow in the PBL, and upper-level anticyclonic outflow; and (b) the present PV inversion system is capable of recovering almost all typical features in a hurricane, provided that diabatic heating and surface friction together with hurricane vortices could be accurately specified.

It should be mentioned that the quasi-balanced flows presented above are obtained from a simulated hurricane that is highly axisymmetric. It is desirable to apply the present PV inversion system to some highly asymmetric storms to see to what extent the above conclusion is applicable. Moreover, in this study we have treated most of the differenced mass and wind fields as unbalanced, propagating inertial gravity waves without providing detailed analysis. In a forthcoming paper, the PV inversion system developed herein will be utilized to separate the unbalanced (wave) from quasi-balanced components of the hurricane flows and then study their individual characteristics and interactions.

Acknowledgments. We would like to thank Dominique Möller, Lloyd Shapiro, Yongsheng Chen, and an anonymous reviewer for their constructive comments, and Mike Montgomery for his helpful discussion. This work was supported by the NSF Grant ATM-9802391, the NASA Grant NAG-57842, and the ONR Grant N00014-96-1-0746.

APPENDIX A

Equations of Atmospheric Motion in *z* Coordinates

Most of the previous PV diagnostic studies used π as a vertical coordinate (e.g., DE91; Shapiro and Franklin 1995; Olsson and Cotton 1997), where π is the Exner function [$\pi = C_p(P/p_0)^\kappa$, $\kappa = R_d/C_p$]. For the convenience of using the multigrid solver of MUDPACK by Adams (1991), it is desirable to adopt the pressure-dependent, pseudoheight z coordinates of Hoskins and Bretherton (1972) that are natural vertical coordinates pointing upward. The variables z and π are related by

$$z = (1 - \pi/C_p)z_a, \tag{A1}$$

where $z_a = (C_p/R_d)H_s$, and $H_s = p_0/\rho_0 g = R_d\theta_0/g$ is the scale height and θ_0 is the reference potential temperature.

The equations of motion for a hydrostatic atmosphere, including the water loading effects, in z coordinates can be written as

$$\frac{\partial u}{\partial t} + u\frac{\partial u}{\partial x} + v\frac{\partial u}{\partial y} + \omega\frac{\partial u}{\partial z} - fv = -\frac{\partial \phi}{\partial x} + F_x,$$

$$\frac{\partial v}{\partial t} + u\frac{\partial v}{\partial x} + v\frac{\partial v}{\partial y} + \omega\frac{\partial v}{\partial z} + fu = -\frac{\partial \phi}{\partial y} + F_y,$$

$$\frac{\partial \phi}{\partial z} = \frac{g}{\theta_0}\theta_\rho,$$

$$\frac{\partial \theta_\rho}{\partial t} + u\frac{\partial \theta_\rho}{\partial x} + v\frac{\partial \theta_\rho}{\partial y} + \omega\frac{\partial \theta_\rho}{\partial z} = \dot{Q}_\rho,$$

$$\frac{\partial u}{\partial x} + \frac{\partial v}{\partial y} + (z_a - z)^{-C_v/R_d}\frac{\partial}{\partial z}[(z_a - z)^{C_v/R_d}\omega] = 0, \tag{A2}$$

where most of the symbols assume their usual meteorological meaning. Because of the importance of water loading in determining the hydrostatic balance in the eyewall of hurricanes (see Zhang et al. 2000), it is highly desirable to include the effects of airborne moisture (i.e., vapor and cloud condensate) and precipitation particles (i.e., rain drop, snow, and hail/graupel) on atmospheric temperature. This is done herein through θ_ρ, which is defined as the virtual potential temperature including the water loading effects

$$\theta_\rho = T_\rho\left(\frac{p_0}{p}\right)^{R_d/C_p} = \theta\frac{1 + q_v/\nu}{1 + q_v + q_{\text{liquid}} + q_{\text{solid}}}, \quad \text{(A3)}$$

where $\nu = R_d/R_v \approx 0.622$; and q_v, q_{liquid}, and q_{solid} represent vapor, liquid, and solid cloud particles, respectively. The diabatic heat rate $\dot{Q}_\rho$ in (A2) is given by

$$\dot{Q}_\rho = \frac{1 + q_v/\nu}{1 + q_v + q_{\text{liquid}} + q_{\text{solid}}}\frac{d\theta}{dt} + \theta\frac{d}{dt}\left(\frac{1 + q_v/\nu}{1 + q_v + q_{\text{liquid}} + q_{\text{solid}}}\right). \quad \text{(A4)}$$

Based on the scale analysis (not shown) and the results of Zhang et al. (2002), the second term on the rhs of (A4) is one order of magnitude smaller than the first term, so the former is omitted in our computation of $\dot{Q}_\rho$.

APPENDIX B

Nondimensionalization of the PV Diagnostic Equations

To efficiently solve for the balanced mass and wind fields, all the variables in the NLB and PV equations need to be nondimensionalized. For this purpose, we define $X = Lx$, $Y = Ly$, $Z = Hz$, $P = p_0 p$, $F = f_0 f$, where the characteristic parameters L and H have a unit of meter, and $p_0 = 10^5$ Pa, $f_0 = 10^{-4}$ s^{-1}. This gives $\Phi = L^2 f_0^2 \phi$ and $\Psi = L^2 f_0 \psi$, $F_x = f_0^2 L f_x$, and $F_y = f_0^2 L f_y$; $\mathbf{f}_r = (f_x, f_y)$. Substituting the above relations into Eqs. (4) and (5) leads to

$$\frac{L^2 f_0^2}{L^2}\nabla^2\phi = \frac{L^2 f_0^2}{L^2}\boldsymbol{\nabla}\cdot(f\boldsymbol{\nabla}\psi) + \frac{L^4 f_0^2}{L^4}2J\left(\frac{\partial\psi}{\partial x}, \frac{\partial\psi}{\partial y}\right) + \frac{f_0^2 L}{L}\boldsymbol{\nabla}\cdot\mathbf{f}_r, \quad \text{(B1)}$$

$$Qq' = \frac{1}{r(Z)}\frac{\theta_0}{G}\left[\left(f_0 f + \frac{L^2 f_0}{L^2}\nabla^2\psi\right)\frac{L^2 f_0^2}{H^2}\frac{\partial^2\phi}{\partial z^2} - \frac{L^4 f_0^3}{L^2 H^2}\left(\frac{\partial^2\psi}{\partial x\partial z}\frac{\partial^2\phi}{\partial x\partial z} + \frac{\partial^2\psi}{\partial y\partial z}\frac{\partial^2\phi}{\partial y\partial z}\right)\right]. \quad \text{(B2)}$$

Since $r(Z) = \rho_0(P/p_0)^{C_v/C_p} = \rho_0 p^{C_v/C_p}$, letting $q' = qp^{C_v/C_p}$ gives

$$Qq = \frac{1}{\rho_0}\frac{\theta_0}{G}\frac{L^2 f_0^3}{H^2}\left[(f + \nabla^2\psi)\frac{\partial^2\phi}{\partial z^2} - \left(\frac{\partial^2\psi}{\partial x\partial z}\frac{\partial^2\phi}{\partial x\partial z} + \frac{\partial^2\psi}{\partial y\partial z}\frac{\partial^2\phi}{\partial y\partial z}\right)\right]. \quad \text{(B3)}$$

Similarly, we can nondimensionalize the hydrostatic equation in (A2) as

$$\frac{L^2 f_0^2}{H}\frac{\partial\phi}{\partial z} = \frac{G}{\theta_0}\Theta\theta. \quad \text{(B4)}$$

If we assume $Q = (\theta_0/\rho_0 G)(L^2 f_0^3/H^2)$ and $\Theta = L^2 f_0^2\theta_0/GH$ as the respective characteristic scales of PV and potential temperature, then Eqs. (B1), (B3), and (B4) will correspond exactly to Eqs. (4′), (5′), and (12), respectively.

REFERENCES

Adams, J., 1993: MUDPACK-2: Multigrid software for approximating elliptic partial differential equations on uniform grids with any resolution. *Appl. Math. Comput.*, **53,** 235–249.

Arnason, G., 1958: A convergent method for solving the balance equation. *J. Meteor.*, **15,** 220–225.

Bishop, C. H., and A. J. Thorpe, 1994: Potential vorticity and the electrostatic analogy: Quasi-geostrophic theory. *Quart. J. Roy. Meteor. Soc.*, **120,** 713–731.

Challa, M., and R. L. Pfeffer, 1980: Effects of eddy fluxes of angular momentum on the model hurricane development. *J. Atmos. Sci.*, **37,** 1603–1618.

Davis, C. A., 1992: Piecewise potential vorticity inversion. *J. Atmos. Sci.*, **49,** 1397–1411.

——, and K. A. Emanuel, 1991: Potential vorticity diagnostics of cyclogenesis. *Mon. Wea. Rev.*, **119,** 1929–1953.

——, and M. L. Weisman, 1994: Balanced dynamics of mesoscale vortices produced in simulated convective systems. *J. Atmos. Sci.*, **51,** 2005–2030.

——, E. D. Grell, and M. A. Shapiro, 1996: The balanced dynamical nature of a rapidly intensifying oceanic cyclone. *Mon. Wea. Rev.*, **124,** 3–26.

Eliassen, A., 1952: Slow thermally or frictionally controlled meridional circulation in a circular vortex. *Astrophys. Norv.*, **5,** 19–60.

Franklin, J. L., S. J. Lord, S. E. Feuer, and F. D. Marks, 1993: The kinematic structure of Hurricane Gloria (1985) determined from nested analyses of dropwindsonde and Doppler radar data. *Mon. Wea. Rev.*, **121,** 2433–2451.

Hoskins, B. J., and F. P. Bretherton, 1972: Atmospheric frontogenesis models: Mathematical formulation and solution. *J. Atmos. Sci.*, **29,** 11–37.

——, M. E. McIntyre, and A. W. Robertson, 1985: On the use and significance of isentropic potential vorticity maps. *Quart. J. Roy. Meteor. Soc.*, **111,** 877–946.

Huo, Z.-H., D.-L. Zhang, and J. R. Gyakum, 1999a: The interaction of potential vorticity anomalies in extratropical cyclogenesis. Part I: Static piecewise inversion. *Mon. Wea. Rev.*, **127,** 2546–2561.

——, ——, and ——, 1999b: The interaction of potential vorticity anomalies in extratropical cyclogenesis. Part II: Sensitivity to initial perturbations. *Mon. Wea. Rev.*, **127,** 2563–2575.

Krishnamurti, T. N., 1968: A diagnostic balance model for studies of weather systems of low and high latitudes, Rossby number less than 1. *Mon. Wea. Rev.*, **96,** 197–207.

Liu, Y., D.-L. Zhang, and M. K. Yau, 1997: A multiscale numerical study of Hurricane Andrew (1992). Part I: Explicit simulation and verification. *Mon. Wea. Rev.*, **125,** 3073–3093.

——, ——, and ——, 1999: A multiscale numerical study of Hurricane Andrew (1992). Part II: Kinematics and inner-core structures. *Mon. Wea. Rev.*, **127,** 2597–2616.

Marks, F. D., R. A. Houze, and J. F. Gamache, 1992: Dual-aircraft investigation of the inner core of Hurricane Norbert. Part I: Kinematic structure. *J. Atmos. Sci.*, **49,** 919–942.

McWilliams, J. C., 1985: A uniformly valid model spanning the regimes of geostrophic and isotropic, stratified turbulence: Balanced turbulence. *J. Atmos. Sci.*, **42,** 1773–1774.

Molinari, J., S. Skubis, D. Vollaro, F. Alsheimer, and H. E. Willoughby, 1998: Potential vorticity analysis of tropical cyclone intensification. *J. Atmos. Sci.*, **55,** 2632–2644.

Möller, J. D., and S. C. Jones, 1998: Potential vorticity inversion for

tropical cyclones using the asymmetric balance theory. *J. Atmos. Sci.,* **55,** 259–282.
——, and M. T. Montgomery, 1999: Vortex Rossby waves and hurricane intensification in a barotropic model. *J. Atmos. Sci.,* **56,** 1674–1687.
——, and L. J. Shapiro, 2002: Balanced contributions to the intensification of Hurricane Opal as diagnosed from a GFDL model forecast. *Mon. Wea. Rev.,* **130,** 1866–1881.
Montgomery, M. T., and J. L. Franklin, 1998: An assessment of the balance approximation in hurricanes. *J. Atmos. Sci.,* **55,** 2193–2200.
Olsson, P. Q., and W. R. Cotton, 1997: Balanced and unbalanced circulations in a primitive equation simulation of a midlatitude MCC. Part II: Analysis of balance. *J. Atmos. Sci.,* **54,** 479–497.
Raymond, D. J., 1992: Nonlinear balance and potential-vorticity thinking at large Rossby number. *Quart. J. Roy. Meteor. Soc.,* **118,** 987–1015.
Reasor, P. D., M. T. Montgomery, F. D. Marks Jr., and J. F. Gamache, 2000: Low-wavenumber structure and evolution of the hurricane inner core observed by airborne dual-Doppler radar. *Mon. Wea. Rev.,* **128,** 1653–1680.
Reed, R. J., M. T. Stoelinga, and Y.-H. Kuo, 1992: A model-aided study of the origin and evolution of the anomalously high potential vorticity in the inner region of a rapidly deepening marine cyclone. *Mon. Wea. Rev.,* **120,** 893–913.
Sasaki, Y. K., and J. A. McGinley, 1981: Application of the inequality constraint in adjustment of superadiabatic layers. *Mon. Wea. Rev.,* **109,** 194–196.
Schubert, W. H., and B. T. Alworth, 1987: Evolution of potential vorticity in tropical cyclones. *Quart. J. Roy. Meteor. Soc.,* **113,** 147–162.
——, S. A. Hausman, M. Garcia, K. V. Ooyama, and H.-C. Kuo, 2001: Potential vorticity in a moist atmosphere. *J. Atmos. Sci.,* **58,** 3148–3157.
Shapiro, L. J., 1996: The motion of Hurricane Gloria: A potential vorticity diagnosis. *Mon. Wea. Rev.,* **124,** 2497–2508.
——, and H. E. Willoughby, 1982: The response of balanced hurricanes to local sources of heat and momentum. *J. Atmos. Sci.,* **39,** 378–394.
——, and M. T. Montgomery, 1993: A three-dimensional balance theory for rapidly rotating vortices. *J. Atmos. Sci.,* **50,** 3322–3335.
——, and J. L. Franklin, 1995: Potential vorticity in Hurricane Gloria. *Mon. Wea. Rev.,* **123,** 1465–1475.
——, and ——, 1999: Potential vorticity asymmetries and tropical cyclone motion. *Mon. Wea. Rev.,* **127,** 124–131.
Sundqvist, H., 1970: Numerical simulation of the development of tropical cyclones with a ten-level model. *Tellus,* **22,** 359–390.
Thorpe, A. J., and C. H. Bishop, 1995: Potential vorticity and the electrostatic analogy: Ertel–Rossby formulation. *Quart. J. Roy. Meteor. Soc.,* **121,** 1477–1495.
Trier, S. B., and C. A. Davis, 2002: Influence of balanced motions on heavy precipitation within a long-lived convectively generated vortex. *Mon. Wea. Rev.,* **130,** 877–899.
Willoughby, H. E., 1979: Forced secondary circulations in hurricanes. *J. Geophys. Res.,* **84,** 3173–3183.
——, 1990: Gradient balance in tropical cyclones. *J. Atmos. Sci.,* **47,** 265–274.
Wu, C.-C., and K. A. Emanuel, 1995a: Potential vorticity diagnostics of hurricane movement. Part I: A case study of Hurricane Bob (1991). *Mon. Wea. Rev.,* **123,** 69–92.
——, and ——, 1995b: Potential vorticity diagnostics of hurricane movement. Part II: Tropical storm Ana (1991) and Hurricane Andrew (1992). *Mon. Wea. Rev.,* **123,** 93–109.
Zhang, D.-L., Y. Liu, and M. K. Yau, 2000: A multiscale numerical study of Hurricane Andrew (1992). Part III: Dynamically induced vertical motion. *Mon. Wea. Rev.,* **128,** 3772–3788.
——, ——, and ——, 2001: A multiscale numerical study of Hurricane Andrew (1992). Part IV: Unbalanced flows. *Mon. Wea. Rev.,* **129,** 92–107.
——, ——, and ——, 2002: A multiscale numerical study of Hurricane Andrew (1992). Part V: Inner-core thermodynamics. *Mon. Wea. Rev.,* **130,** 2745–2763.